Electric force on plasma ions and the momentum of the ion-neutrals flow

G. Makrinich[1], A. Fruchtman[1], D. Zoler[1*] and R. Boxman[2]

[1]*Plasma Laboratory, H.I.T. - Holon Institute of Technology, Holon 58102, Israel.*

[2]*Electrical Discharge and Plasma Laboratory, Tel Aviv University, Tel Aviv, Ramat-Aviv, 69978, Israel.*

gennady@hit.ac.il

The electric force on ions in plasma and the momentum flux carried by the mixed ion-neutral flow were measured and found equal. The experiment was performed in a direct-current gas discharge of cylindrical geometry with applied radial electric field and axial magnetic field. The unmagnetized plasma ions, neutralized by magnetized electrons, were accelerated radially outward transferring part of the gained momentum to neutrals. Measurements were taken for various argon gas flow rates between 13-100 Standard Cubic Centimeter per Minute (SCCM), for a discharge current of 1.9 A and a magnetic field intensity of 136 G. The plasma density, electron temperature and plasma potential were measured at various locations along the flow. These measurements were used to determine the local electric force on the ions. The total electric force on the plasma ions was then determined by integrating radially the local electric force. In parallel, the momentum flux of the mixed ion-neutral flow was determined by measuring the force exerted by the flow on a balance force meter (BFM). The maximal plasma density was between 6×10^{10} cm^{-3} and 5×10^{11} cm^{-3}, the maximal electron temperature was between 8 eV and 25 eV and the deduced maximal electric field between 2200 V/m and 5800 V/m. The force exerted by the mixed ion-neutral flow on the BFM agreed with the total electric force on the plasma ions. This agreement showed that it is the electric force on the plasma ions that is the source of the momentum acquired by the mixed ion-neutral flow.

*On leave from Propulsion Physics Laboratory, Soreq Nuclear Research Center, Yavne 81800, Israel.

This manuscript was accepted by J. Appl. Phys. Click here to see the version of record.

I.Introduction

Quasi-neutral plasma can be accelerated by magnetic pressure, when a current flows across a magnetic field and the net force per unit volume on the plasma is $\vec{j} \times \vec{B}$, the cross product of the current density $\vec{j}$ and the magnetic field $\vec{B}$ (in a crossed electric and magnetic field configuration). Indeed, the $\vec{j} \times \vec{B}$ force is used for accelerating quasi-neutral plasmas in electromagnetic thrusters, such as the Hall thruster (HT) [1], [2], [3] the Highly Efficient Multistage Plasma Thruster (HEMP-T) [4], the Helicon Hall Thruster (HHT) [5], [6] and the Magneto-Plasma Dynamics (MPD) thruster [7]. Electrodeless thrusters also employ magnetic pressure, [8], [9] [10], [11]. Magnetic pressure is also used for materials modification (for example, magnetron sputtering systems and vacuum arc sources) [12], [13], [14], [15], in radiation sources (e.g. pinches) [16], in MHD generators [17] and in plasma opening switches [18]. Ion-neutral collisions can affect thrust generation, either through gas heating [19] or through momentum enhancement as is explored here.

The momentum delivered to a mixed ion-neutral flow by an electric force can be enhanced if ions collide with neutrals during the acceleration. That enhancement, known for un-magnetized non-neutral ion flow [20], [21], [22], [23], [24], has been demonstrated and measured in recent years for partially-ionized quasi-neutral magnetized plasma accelerated in a $\vec{j} \times \vec{B}$ configuration in a Radial Plasma Source (RPS) [25], [26] [27], a configuration in which plasma acceleration has been studied in the past [28]. Later, similar enhancement of force on a surface in plasma due to ion-neutral collisions was also measured [29], [30]. In the RPS, shown in Figure 1 and described in detail in the next sections, plasma is generated between two parallel coaxial circular discs. The plasma ions are accelerated radially outward by an applied electric field, while the electron motion is

impeded by a magnetic field which is applied in the axial direction, perpendicular to the electric field. If the neutrals density is high enough, the ions collide with neutrals during their acceleration by the electric field. In the experiments [25], [26] [27], the momentum flux, carried by the mixed ion-neutral flow after the flow has crossed the electric potential drop, was determined by measuring the force that the flow exerted on a Balance Force Meter (BFM). The momentum flux was so determined because the force exerted on the BFM should be equal to the momentum flux carried by the flow. The momentum flux carried by the flow was expected to result from the electric force on the plasma ions. Therefore, by measuring the force exerted on the BFM, the electric force on flow, in fact on the ion flow, was expected to be found. This measured (assumed electric) force on the ion flow was found in [25], [26] [27], to be enhanced relative to the electric force on the same ion flow that would have crossed the potential drop without collisions with neutrals. The enhancement of the (assumed electric) force was shown to be proportional to the square root of the calculated number of collisions with neutrals an ion experiences as it crosses the potential drop.

In these previous studies [25], [26] [27], only the **total** assumed-electric force was evaluated by the BFM measurements. The main objective of the present work was to show that indeed it is the electric force on the plasma ions that delivers the momentum to the mixed ion-neutrals flow. This is shown here by measuring the **local** electric force on the ions in the RPS and by comparing the integrated measured local electric force with the total assumed-electric force that was evaluated by the force on the BFM.

For finding the local electric force on the ions in the RPS, the radial profiles of the plasma potential and the plasma density along the acceleration have been deduced from measurements by a planar Langmuir probe and an emissive probe. A method for deducing

the plasma potential and the plasma density from the probe measurements was used, which is based on our theoretical model [31]. The method is presented in the Appendix. That method and the deduced plasma potential and plasma density were briefly reported previously [32]. Here, the radial profiles of the deduced plasma potential and plasma density are presented in more detail. The local electric force is then calculated employing those radial profiles, as follows. Using the profiles of the plasma potential, the electric field is evaluated. The evaluated electric field and plasma density are used to determine the local electric force per unit volume on the ions. By integrating this local electric force across the volume where the electric field was applied, the total electric force on the plasma ions is calculated. This total electric force agrees with the BFM measurements. This agreement shows that it is the electric force on the plasma ions that is the source of the momentum acquired by the mixed ion-neutral flow.

Because of the azimuthal symmetry of the RPS, the net thrust delivered by the ejected plasma is zero. However, the enhancement of the local electric force by ion-neutral collisions in the RPS is the same as in a thruster configuration. In addition, diagnostics using probes is easier to implement in a RPS configuration, being our reason for choosing the RPS for the current study.

In Section II, the method of deducing from the measured quantities the local and total electric force, the momentum flux carried by the mixed ion-neutral flow and the electron pressure is explained. In Section III, the experimental setup and measurements procedures are described. These include the RPS, the diagnostic system and the measurements procedure. The way the probe measurements are used to deduce the plasma parameters and the plasma potential is explained. In Section IV, the measurements of the plasma parameters are described. In Section V, the deduced-from-measurements radial

This manuscript was accepted by J. Appl. Phys. Click here to see the version of record.

profiles of the plasma potential, the electron temperature and the plasma density are presented. In Section VI, the evaluated radial profiles of the electron pressure and of the electric field are shown. In Section VII, the total electric force is obtained by the radial integration of the local electric force. This obtained total electric force is shown to agree with the momentum flux carried by the mixed ion-neutral flow, a momentum flux that is evaluated from the BFM measurements. The enhancement of the electric force relative to the electric force on collisionless ions is discussed. Finally, we summarize in Section VIII.

II. The method of deducing the electric force

In this section the method of deducing from measurements the electric force on ion flow in the RPS is explained. The RPS, shown in Figure 1, is explained in detail in Section III. Here, a brief description of the physical processes is given. The RPS is composed of two parallel coaxial disks, separated by a distance h. A partially - ionized plasma fills the space between the disks. The volume between the two coaxial disks is the acceleration channel. A radial electric field E_r, applied along the acceleration channel between $r = r_a$ and $r = r_b$, accelerates ions radially outward. Here, r denotes the distance from the RPS axis, r_a and r_b are the distances of the anode and of the BFM from the RPS axis, respectively (these distances are also shown in Figure 1). An axial magnetic field B_z is applied perpendicular to the electric field, of such intensity that electrons are magnetized while ions are unmagnetized. The electric force on the ions delivers to them momentum, a part of that momentum is transferred to the neutrals through ion-neutral collisions. The distributions of the electric field and of the ion density in the plasma are determined by the coupled dynamics of ions and electrons. A full analysis of both ion and electron dynamics (ionization, recombination, and different kind of collisions) that determines the electric field and the plasma density distributions, is not made here. Instead, in the calculations in

This manuscript was accepted by J. Appl. Phys. Click here to see the version of record.

this section, the electric field and the plasma density were taken as known. Later in the paper, the local electric field and plasma density are deduced from the measurements.

The local electric force on the ions, dF_{El}, is

$$dF_{El} = n_i e E_r dV, \tag{1}$$

where n_i is the (singly-charged) ion density, e is the elementary charge and dV is a unit volume. The electric force per a small azimuthal angle $\Delta\theta$ along the acceleration channel is

$$F_{El}(r, \Delta\theta) = \Delta\theta h \int_{r_a}^{r} n_i e E_r r' dr'. \tag{2}$$

Cylindrical coordinates have been used. The total electric force on the plasma ions that together with neutrals compose the mixed ion-neutral flow hitting the BFM is now calculated. The small angle of the flow hitting the BFM is $\Delta\theta = c/r_b$, c is the width of the BFM (in the azimuthal direction of the RPS). Therefore, F_E, the total electric force on the plasma ions, is

$$F_E \equiv F_{El}\left(r_b, \frac{c}{r_b}\right) = \frac{c}{r_b} h \int_{r_a}^{r_b} n_i e E_r r dr. \tag{3}$$

The radial electric field E_r was determined in the experiment as the derivative with respect to r of the measured electric potential. The plasma density n_i was also measured. Therefore, the integral in Equation (**3**) can be evaluated based on the measured E_r and n_i and the electric force can be deduced.

The total electric force F_E can be evaluated by its relation to F_{BFM}, the force that the mixed ion-neutral flow exerts on the BFM. This evaluation is now described.

The momentum flux carried by the mixed ion-neutral flow reaching the end of the acceleration channel that hits the BFM is

This manuscript was accepted by J. Appl. Phys. Click here to see the version of record.

$$F_{mf} = \mathrm{m}_i \Gamma_{flow} \upsilon_{BFM}. \quad (4)$$

Here, Γ_{flow} is the particle flux of the mixed ion-neutral flow and υ_{BFM} is the average velocity of the flow, both upon hitting the BFM, and m_i is the ion mass. The measured force on the BFM by that mixed ion-neutral flow, F_{BFM}, equals this momentum flux (which was not measured)

$$F_{BFM} = F_{mf}. \quad (5)$$

The momentum flux F_{mf} of ions and neutrals in the flow is generated by the above analysed F_E, the electric force on the ions while they are in the plasma. Therefore,

$$F_{mf} = F_E. \quad (6)$$

From Equations (5) and (6) it is expected that

$$F_E = F_{BFM}. \quad (7)$$

Our purpose in the paper is to verify that indeed Equation (7) is satisfied.

III. Experimental setup

A. Plasma source

The RPS was located at the center of a vacuum chamber, which was pumped to a base pressure of 0.01 mTorr prior to the experiment [25]. As is shown in Figure 1, the RPS was made of a cylindrical body and a cathode. The body consisted of an iron core, a magnetic-field generating solenoid, a gas distributor, a ceramic insulator, and a molybdenum anode, and. The iron core consisted of a central rod and two outer parts of a disk shape (an upper part and a lower part in Figure 1). The central rod was of 5 mm in radius and was connected with the two outer parts of radius $r_{\mathrm{m}} = 40$ mm, thus the edge of the RPS body was located at $r_{\mathrm{m}} = 40$ mm as well. The solenoid was wrapped around the central rod of the iron core. The ceramic insulator was composed of two coaxial annular flat disks and an axial segment glued together to form a discharge chamber. The ceramic

insulator was prepared from Al_2O_3 ceramic parts that were glued together by a mixture of Al_2O_3 powder and silicate glue. The outer diameters of the two coaxial annular flat disks were 77 mm, and the inner diameters were 30 mm. The length of the axial segment which established the distance between the two disks was $h = 5$ mm. The molybdenum cylindrical anode was placed between the two disks; it was of $2r_a = 48$ mm in diameter, 4.5 mm in width, and 0.25 mm in thickness. The solenoid was composed of 600 windings of copper wire of 0.5 mm in diameter. The generated magnetic field in the central plane, the plane that is at equal distances from the two ceramic disks, was maximal near the edges of the iron core. As is seen in Figure 1, the ceramic insulator, the solenoid, and the iron core had the same axis of symmetry. The empty cylindrical volume between those three parts (see Figure 1) distributed the working gas, which was injected into this volume through holes in the ceramic insulator. There were 8 holes, 2 mm in diameter each, which were equally spaced azimuthally at 45 degrees between each two neighbouring holes.

A cathode, located at $r_c = 80$ mm from the RPS axis, supplied electrons for neutralizing the ion current. The electrons were thermionically emitted from the cathode, which was heated by a heating coil comprised of five-turns of 0.5 mm diameter of tungsten wire, 10 mm in diameter and 15 mm in height. The heating coil was energized by a dc current of 19 A. For reducing the heating of other parts of the source, the loop was positioned inside a molybdenum cylinder of 25 mm diameter, 45 mm height, and 0.25 mm thickness. The cathode was also supplied by working gas with a flow rate of 4 SCCM.

The RPS operates in the following manner. An iron core generates an axial magnetic field B_z between the anode and the cathode. A gas distributor introduces gas into the region between the anode and the cathode. When a voltage is applied between the anode and the cathode, the magnetic field impedes the motion of the electrons along E_r towards

This manuscript was accepted by J. Appl. Phys. Click here to see the version of record.

the anode. The electrons drift azimuthally around the axis, carrying an azimuthal current j_θ. The electron flow is then axisymmetric, even though the cathode itself is not axisymmetric. The outward radial electric field E_r accelerates the unmagnetized ions outward. The ions collide with neutrals during their acceleration by the electric field. The discharge is ignited through gas ionization by electrons emitted from the cathode. The cathode also provides electrons that neutralize the ion current exiting the PRS, after being accelerated.

The measurements were taken for fixed discharge current of 1.9 A, and fixed magnetic field, the maximum on the middle plane of 136 G. Argon was used in all the experiments. The gas flow rates for which measurements were taken were 13, 30, 50, and 100 SCCM and the corresponding pressure in the vacuum chamber was 2.5, 4.3, 6.6, and 11.5 mTorr, respectively.

B. Diagnostic system

The diagnostic system included probes (shown in Figure 2) and the above mentioned BFM (shown in Figure 1). A planar probe, P1, and an emissive probe were used to measure the plasma parameters and the plasma potential inside the RPS. All these inner RPS measurements were taken along the same radial line on the central plane (and approximately opposite azimuthally to the cathode location). Probe P1, a tantalum planar probe of dimensions 2.5×7mm^2 and thickness of 0.25 mm, was used to measure the ion saturation current in the plasma. The collecting surface of P1 was in the (r, θ) plane, parallel to the radial ion flow.

The emissive probe consisted of a filament that was connected at both its ends to two copper wires isolated from the plasma by two alumina tubes. The filament was a tungsten wire of diameter d_{em}= 0.01 cm and of length l_{em} =1 cm. The axis of the filament

was placed on the middle plane of the RPS, so that a line perpendicular to that axis on that plane intersected both the filament center and the RPS axis. The filament was heated by a DC current and the probe floating potential reached saturation at a heating current of 2.0 - 2.5 A, while the voltage along the filament was 3 - 4 V. The measurements by the emissive probe were taken along the same radial line where the P1 measurements were taken.

For the influence of the magnetic field on the emissive probe to be small, the probe radius should be much smaller than the electron Larmor radius, the condition for that to happen is that $1 \ll 4.8\sqrt{T_e}/(d_{em}B)$ [33], [34], (B is in Gauss, T_e is in eV, and d_{em} is in cm). In our experiment, the measured parameters were $B \leq 136$ G., $T_e \geq 5$ eV, so that the above condition was satisfied.

A cylindrical Langmuir probe, a tungsten wire of 0.25 mm diameter and of 5 mm length, was positioned 5 mm downstream from the emissive probe, as shown in Figure 2. In all experiments, no change was found in the floating potential measured by the cylindrical Langmuir probe due to the electron emission from the emissive probe.

The momentum flux carried by the flow was evaluated by measuring the force exerted by that flow on a sensing plate of the BFM. Similar to other impact force meters [29], [30], [35], [36], [37], [38], [39], [40], [41], the BFM measures the force by balancing its torque with the torque of some other measured force. The design and the calibration of the BFM were described previously in more detail [27].

A force is exerted on the BFM by the neutral gas that flows out of the RPS even when there is no discharge [26]. The change in the force exerted by the mixed ion-flow due to the discharge, F_{BFM}, was found as the difference between two forces

$$F_{BFM} = F_{on} - F_{off}\,, \tag{8}$$

This manuscript was accepted by J. Appl. Phys. Click here to see the version of record.

where F_{on} is the force measured when the RPS discharge is on and F_{off} is the force measured when the discharge is turned off. The BFM was positioned at $r_b = 70$ mm, on the radial line along which all measurements were taken. From the inaccuracies of F_{on} as 5% and of F_{off} as 3.5%, we determine the inaccuracy of F_{BFM} as 6%.

In addition, another planar probe, called here P2, was used as in Ref. [26], to measure the radially outward ion current outside the RPS (at $r = r_b$), therefore its collecting surface was perpendicular to the radial ion flow (see Figure 2). The measured ion current was used to evaluate the force enhancement relative to the case without collisions, the effect studied in Refs [25], [26] [27].

IV. Measurements in the plasma

In this section we describe the measurements inside the RPS. Three measurements were taken at each radial location. The floating potential of the emissive probe was measured twice. The floating potential when the probe was cold and non-emitting was denoted V_f. The floating potential when the probe was sufficiently heated for space-charge limited emission was denoted V_{ef}. This V_{ef} (which is higher than V_f) is a rough estimate of the plasma potential V_p. A more accurate evaluation of V_p is presented in Section V. The third measurement was of the ion saturation current of P1, denoted I_{is}.

Figure 3 shows the measured V_f and V_{ef} (relative to the grounded cathode, $V_c = 0$) at various distances from the RPS axis, $r_2 = 28$ mm, $r_3 = 32$ mm, $r_4 = 38$ mm, $r_5 = 46$ mm, and $r_6 = 70$ mm, and at the anode position, denoted as $r_1 \equiv r_a = 24$ mm. At each location, V_f and V_{ef} are shown for two gas flow rates, 13 SCCM and 100 SCCM. Both V_f and V_{ef} generally decreased from the anode towards the edge of the RPS body. In a specific mode of the emissive probe operation, either cold or hot probe, the floating potential was higher for a lower gas flow rate.

This manuscript was accepted by J. Appl. Phys. Click here to see the version of record.

Figure 4 shows the ion saturation current I_{is} of P1 for the four different gas flow rates mentioned above, 13, 30, 50, and 100 SCCM, at various distances from the RPS axis of symmetry. As is seen in Figure 4, for 30, 50, 100 SCCM, the ion saturation current was much larger near the anode than near the edge of the RPS body. For these three gas flow rates, there was a maximum of the ion saturation current at $r \cong 30$ mm, about halfway between the anode and the edge of the RPS body. For the 13 SCCM gas flow rate, the maximum of the ion saturation current was at the edge of the RPS body. The ion saturation current increased with the gas flow rate.

V. Deducing the plasma potential, electron temperature and plasma density

Following the method described in the Appendix, the plasma potential V_p, the electron temperature T_e and the plasma density n_i were deduced using the measured V_f, V_{ef} and I_{is}. Maxwellian energy distribution was assumed for the electrons, although it may not be accurate when the gas flow rate is low. The radial profiles of V_p, T_e and n_i for the four gas flow rates, found by solving Equations (A1), are shown in Figures 5, 6, and 7. Also shown is the anode potential, V_a, which was equal to the discharge voltage, $V_d \equiv V_a - V_c$, since $V_c = 0$.

The plasma potential V_p, shown in Figure 5, decreased from the anode towards the cathode and was in the range from 22 V to 105 V. At the nearest point to the anode where the measurements were taken, the plasma potential was found to be equal, within the error bar, to the anode potential (presented as separate points in the figure at $r = r_a = 24$ mm). At a distance of $r = r_b = 70$ mm from the RPS axis, where the BFM was later positioned, the plasma potential was about 25 V.

Figure 5 also shows the effect of the gas flow rate on the plasma potential when, as in our experiment, the discharge current and the magnetic field intensity are kept constant.

This manuscript was accepted by J. Appl. Phys. Click here to see the version of record.

It is seen in the figure that V_p decreases at all locations, as the gas flow rate increases. The measured potential drop across the plasma, $V_p(r = 28\text{ mm}) - V_p(r = 70\text{ mm})$, decreases with the gas flow rate. The discharge voltage (here, V_a) decreases with the gas flow rate as well. The discharge voltage was 106, 82, 74, and 62 V for the gas flow rates 13, 30, 50, and 100 SCCM respectively.

It is seen in Figure 5 that for all four gas flow rates, most of the plasma potential drop is between $r \cong 28$ mm and $r \cong 46$ mm, away from the anode and the cathode. The potential drop at the vicinity of the anode and outside the RPS, seem to be small (except possibly in a cathode sheath). Most of the discharge voltage falls across the plasma. The electric field, derived from the potential profiles, is discussed in Section VI.

The electron temperature, T_e, shown in Figure 6, decreased from the anode towards the cathode. In the various experiments, the electron temperature varied between 3 eV and 25 eV. At the anode vicinity, the highest temperature was $T_e = 25$ eV for 13 SCCM and the lowest temperature at the anode vicinity was 8 eV for 100 SCCM. Most of the measured temperature drop was between $r \cong 28$ mm and $r \cong 46$ mm, approximately in the same region where most of the potential drop was, as was shown in Figure 5.

The radial profile of the plasma density n_i is shown in Figure 7. In the various experiments, the plasma density varied between 2×10^{10} cm^{-3} and 5×10^{11} cm^{-3}. For 30, 50 and 100 SCCM, the plasma density decreased from the anode towards the cathode. The plasma density for the 13 SCCM gas flow rate was different; it increased from the anode towards the cathode, reaching a maximum outside the RPS body near its outer edge. For a higher gas flow rate, the plasma density was higher.

VI. Radial profiles of the electric field and the electron pressure

As explained in detail in Section II, in order to calculate dF_{El}, the local electric force on the ions, the ion density n_i and the radial electric field E_r have to be known. Using the deduced plasma potential (Figure 5), the radial electric field E_r was determined as minus the derivative of the plasma potential with respect to r. As described in Section V and presented in Figure 5, the potential was deduced in five radial locations inside the plasma and was also known at the anode, a total of six radial locations. The electric field was therefore specified at five radial locations, each at the middle between two neighbouring radial locations where the potential was known. The deduced electric field is presented in Figure 8 for the four gas flow rates. It is seen in the figure that E_r varies between - 500V/m to 5800 V/m (±500 V/m). The electric field increased with r from the anode, reached a maximum at $r \approx 35$ mm and then decreased toward the cathode. The dependence of the electric field on r was similar for different gas flow rates, but the electric field was lower when the gas flow rate was higher. The deduced maximal electric field was 5800, 3900, 3100 and 2200 V/m for the gas flow rates 13, 30, 50, and 100 SCCM respectively. Near the anode the electric field was very small, possibly even pointing towards the anode (for the gas flow rate 100 SCCM).

Figure 8 also shows the measured radial profile of the axial magnetic field (dashed line). It is seen that the profiles of the electric field and of the magnetic field have some similarity. The electric field is higher in regions where the magnetic field is higher and the location of the maximum of the electric field is close to the location of the maximum of the magnetic field, similar to what was measured for the Hall thruster [42] [2]. As mentioned above, the intensity of the magnetic field was not varied in the experiment.

This manuscript was accepted by J. Appl. Phys. Click here to see the version of record.

The Larmor radius of a collisionless ion accelerated by the electric field across the magnetic field of intensities as presented above is much larger than the anode-cathode distance. If the ion collides with neutrals, as in the experiments here, then its mean free path between collisions is much smaller than its Larmor radius. Both collisionless and collisional ions are unmagnetized in our experiment and they gain momentum from the electric force only.

From the measured profiles of the electron temperature in Figure 6 and of the ion density in Figure 7, profiles of the electron pressure, $p_e = k_B n_e T_e$, were calculated, assuming $n_e = n_i$ (k_B is Boltzmann constant). The radial profile of the electron pressure is shown in Figure 9. In the various experiments, the electron pressure varied between 0.03 Pa and 0.6 Pa. The electron pressure was higher near the anode than it was near the edge of the RPS body, except for the gas flow rate of 13 SCCM, for which p_e hardly varied along the acceleration channel. The electron pressure was higher for a higher gas flow rate. The maximal p_e for the gas flow rate of 13 SCCM was 0.1 Pa only, much lower than the maximal p_e for the three higher gas flow rates. The higher p_e for a higher gas flow rate was a result of n_e being higher, even though T_e was lower.

VII. The total electric force on the plasma ions and the force on the BFM

Figure 10 shows forces as a function of gas flow rate. Two of the forces are F_{BFM} and F_E, described in Section II. As stated in Section II, our purpose is to examine whether the two forces, F_{BFM} and F_E, are equal. Two other forces that are shown in Figure 10 will be discussed later.

The force exerted by the mixed ion-neutral flow, F_{BFM}, was measured as described in Section IIIB. The force F_{BFM} was found to be 0.039, 0.046, 0.056 and 0.087 mN for the

This manuscript was accepted by J. Appl. Phys. Click here to see the version of record.

gas flow rates of 13, 30, 50 and 100 SCCM, respectively. Incidentally, the force F_{off} was 0.008, 0.017, 0.025, and 0.042 mN, respectively.

The total electric force on the plasma ions, F_E, was calculated using Equation (3). The plasma potential and ion density in the plasma, obtained at $r = r_j$, $j = 2, \dots, 6$, for various gas flow rates, were used for the calculation. At the anode, we write $V_p(r_1) = V_a$, and the ion density was assumed zero, $n_i(r_1) = 0$. In each interval between two neighbouring radial locations where measurements were taken, the electric field was assumed constant and the ion density was assumed to vary linearly with r. For $r_j < r < r_{j+1}$, when $j = 1, \dots, 5$, the constant electric field was taken as

$$E_{rj}(r) = -\frac{[V_p(r_{j+1}) - V_p(r_j)]}{(r_{j+1} - r_j)}, \tag{9}$$

and the ion density as

$$n_{ij}(r) = n_i(r_j) + [n_i(r_{j+1}) - n_i(r_j)]\frac{(r - r_j)}{(r_{j+1} - r_j)}. \tag{10}$$

Note that in Equation (10) j only is an index. With these electric field and ion density, the electric force in each interval was evaluated as

$$F_{Ej} = \frac{c}{r_b} h E_{rj}(r) \int_{r_j}^{r_{j+1}} e n_{ij}(r) r dr, \tag{11}$$

The width of the sensing plate of the BFM in the azimuthal direction was $c = 20$ mm. The total electric force on the plasma ions, as defined in Equation (3), was calculated as the sum of electric forces in the five intervals,

$$F_E = \sum_{j=1}^{5} F_{Ej}. \tag{12}$$

The total electric force F_E was found to be 0.032, 0.062, 0.073 and 0.095 mN for gas flow rates of 13, 30, 50 and 100 SCCM, respectively. Taking into account the inaccuracy in the measured V_p, n_i, and r, we determine the inaccuracy of F_E as 15%.

Both forces, F_{BFM} and F_E, are shown in Figure 10 to increase with gas flow rate. The two forces are of a similar magnitude. Nevertheless, it looks from Figure 10 as though there is still a noticeable difference between the two forces. For the three higher gas flow rates, the total electric force on the ions, F_E, is clearly higher than , F_{BFM}, the force measured by BFM, while for gas flow rate of 13 SCCM, F_E is slightly smaller than F_{BFM}. Let us discuss possible explanations for these differences.

It is reasonable that the momentum flux of the mixed ion-neutral flow is smaller than the electric force on the ions. This is because some of momentum acquired by the flow in the radial direction may be lost upon collisions of energetic ions or electrons with the disks. The measured lower F_{BFM} could be a result of this momentum loss. As mentioned above, for gas flow rate of 13 SCCM, F_E was not higher than F_{BFM}, rather it was slightly smaller. However, if the gas density is small, the number of scattering ion-neutrals collisions is small, and the momentum loss at wall collisions is expected to be small. Therefore, F_{BFM} that is not smaller than F_E for the lower gas flow rate is not surprising.

We should note in calculating F_{Ej} in Equation (11), it was assumed that the ion density was uniform axially between the disks. The value of the ion density was deduced from $n_i(r_j)$ that was obtained from the Langmuir probe that was placed at the middle plane between the disks. However, the plasma density is expected to be lower near the walls. Therefore, the actual electric force on the plasma ions should be somewhat smaller than F_E deduced from Equation (12). This effect should hold though for all four gas flow rates.

We showed that there is a good agreement between F_{BFM} and F_E, which was our purpose in this paper. Therefore, the measured F_{BFM} equals the total force on the plasma ions, confirming our assumption in Refs [25], [26], [27].

The electric force on the ions should be approximately equal in the quasi-neutral plasma to the electric force on the electrons. As stated in Section II, the electric force on the magnetized electrons should be balanced by the magnetic force. The contribution of the electron pressure in our experiment is expected to be small. Here, we estimate the contribution of the electron pressure. Thus, in addition to evaluating F_{BFM} and F_E, the force due to electron pressure, denoted as F_{pe}, was also evaluated. This force was estimated as $F_{pe} = p_{emax}\frac{c}{r_b}r_s h$, where r_s is the distance from the RPS axis, different for different gas flow rates, at which the electron pressure had its maximal value p_{emax}. It was found that F_{pe} was 0.004, 0.019, 0.019 and 0.025 mN for gas flow rates of 13, 30, 50 and 100 SCCM, respectively. Taking into account the inaccuracy in the measured T_e, n_i, and r_s, we determine the inaccuracy of F_{pe} as 15%. The evaluated F_{pe} is also presented in Figure 10. It is seen in Figure 10 that F_{pe} was significantly lower than F_{BFM}, $F_{pe} < 0.25F_{BFM}$, so that the electron pressure is not the main source of F_{BFM}. Thus, we conclude that, as expected, the force due to the electron pressure does not balance the electric force on the electrons rather it is the magnetic force on the electrons.

The agreement between the force deduced from the BFM measurements and the force deduced from the local plasma density and electric field shows that the dominant mechanism for delivering momentum to the mixed ion-neutrals flow is the electric force.

We now discuss the relation between the electric force, the ion current and the discharge voltage. In our previous studies [25], [26], [27], the electric force on the ions was

This manuscript was accepted by J. Appl. Phys. Click here to see the version of record.

found to be enhanced by collisions with neutrals relative to the electric force on the same ion flow that would have crossed the potential drop without such collisions. Enhancement was also found in experiments in which force exerted on a surface in a plasma was determined [29], [30]. The mechanism of enhancement was explained in [25], [26], [27]. If ions are slowed down by collisions with neutrals, their residence time in the acceleration region is increased the electric force is felt by the ions for a longer time, thus the electric force on the ion flow is larger. The momentum delivered to the ion, the product of force and residence (or transit) time, is larger than without collisions. A second explanation was that when a certain kinetic energy is delivered to a larger mass, not only to ions but also to neutrals, the momentum is larger. This enhancement of the electric force is examined also here. For that, the maximal electric force, F_{cl}, that can be exerted by the plasma ions accelerated by the electric field, if they are collisionless, is evaluated. The maximal electric force for collisionless ions is $F_{cl} = \mathrm{m}_i \Gamma_F v_0$, where $\Gamma_F = \left(A_F/A_{p2}\right) I_i/e$ is the radially-outward ion flux onto the BFM (A_F and A_{p2} are the RPS-facing areas of the BFM and of the Langmuir probe P2, respectively, and A_F/A_{p2} =1.2). Also, $v_0 = \sqrt{2eV_{ac}/\mathrm{m}_i}$, $V_{ac} = V_d - V_p(r_b)$ being the potential difference between the anode and the BFM. The radial ion current, I_i, measured by the probe P2, was 4.2, 4.5, 5.2, and 5.0 mA, and the corresponding F_{cl} was 0.041, 0.037, 0.040 and 0.034 mN, for gas flow rates of 13, 30, 50 and 100 SCCM, respectively. Taking into account the inaccuracies in the measured V_p, I_i, A_F and A_{p2}, we determine the inaccuracy in F_{cl} as 12%. The evaluated F_{cl} is also presented in Figure 10. This maximal electric force for collisionless ions, F_{cl}, was approximately the same for 13, 30 and 50 SCCM and somewhat smaller for 100 SCCM. For 13 SCCM, F_{BFM} was similar to F_{cl}, while for the three higher gas flow rates, F_{BFM} was larger than F_{cl}. Thus, it looks as

This manuscript was accepted by J. Appl. Phys. Click here to see the version of record.

though the electric force was enhanced for the higher gas flow rates relative to the force on collisionless ions.

We now examine the suggestion that the enhancement of the electric force here observed was due to ion-neutrals collisions. The mean free path of ion-neutral collision is $\lambda = 1/(\sigma N)$. Here, σ is the total collision cross section, the sum of cross sections of elastic and charge exchange collisions (with a characteristic value $\sigma \approx 80\times10^{-20}$m^2 for argon [43]) and N is the neutrals density. Charge-exchange collisions are efficient in transferring momentum from ions to neutrals. Using the calculated N for 2.5 mTorr (corresponding to 13 SCCM) and assuming (for all gas flow rates) that the gas temperature is 300 K, we find that $\lambda \approx 0.015$ m. Examining Figure 5, we find that for all gas flow rates, the radial length of the region in the acceleration channel, where most of the applied voltage drops, is $a \approx 0.015$ m, about the same as λ. Therefore, ions rarely collide with neutrals as they are accelerated and it is reasonable that $F_{BFM} \cong F_{cl}$ for this gas flow rate. It is also seen in Figure 10 that F_{BFM}/F_{cl} increases with the gas flow rate (and with the gas pressure). If ion-neutrals collisions are the source of electric force enhancement, this observed increase of F_{BFM}/F_{cl} with pressure is expected, as ions collide more often when the gas pressure is higher. For gas flow rate of 100 SCCM and a corresponding pressure 11.5 mTorr, the force enhancement was $F_{BFM}/F_{cl} \cong 2.5$. For that pressure, the mean free path is smaller, $\lambda \cong 0.003$ m and $a/\lambda \cong 5$. The enhancement is expected to be proportional to $\sqrt{a/\lambda} \cong 2.3$, which close to the calculated F_{BFM}/F_{cl}, mentioned above. The measured enhancement of the electric force is thus consistent with the enhancement by ion-neutrals collisions. The enhancement of the electric force was already described in a model and checked experimentally systematically [27]. Here, for the first time the electric force was further evaluated by local measurements.

VIII. Summary

In this paper we showed that in a configuration typical to plasma thrusters in which ions are unmagnetized, it is the electric force on the ions that delivers the momentum to a mixed ion-neutrals flow exiting a discharge. Two forces were compared in experiments in our radial plasma source (RPS). The first force was the electric force on the plasma ions, evaluated by the measured electric potential and plasma density along the RPS accelerating channel. The second force was that exerted on a Balance Force Meter (BFM) outside the RPS by the mixed ion-neutral flow outward of the plasma source. The two forces were approximately equal for various gas flow rates (when the force by the gas flow without a discharge was extracted). Since the force measured by the BFM equals the momentum flux carried by the mixed ion-neutral flow impinging on the BFM, it was concluded that the electric force was the source of the momentum gained by the flow.

For local measurements of the ion density, the electron temperature and the plasma potential, we used a Langmuir probe and an emissive probe, applying an analysis of the emissive probe. The force due to the electron pressure was found to be considerably smaller than the electric force, indicating, as expected, that the electric force on the electrons is balanced by the magnetic force.

As in our previous experiments about the RPS [25], [26], [27], the electric force on the ion flow was also shown here to be enhanced by ion-neutrals collisions. It has been suggested in [27], [44], that this enhancement can be used for developing a high thrust-power ratio thruster. The RPS geometry is not suitable for a thruster, since, because of the azimuthal symmetry, the net thrust by the radial flow is zero. A modified configuration in which a net thrust is delivered, and in which the electric force enhancement is implemented, is currently under investigation.

Acknowledgments

The authors thank Prof. Yakov Krasik, Dr. Yevgeny Raitses and Prof. Isaak Beilis for helpful discussions. This research has been supported by the Israel Science Foundation (Grant no 765/11).

References

[1] A. I. Morozov, Yu. V. Esipchuk, G. N. Tilinin, A. V. Trofimov, Yu. Sharov, and G. Ya. Shchepkin, *Sov. Phys. Tech. Phys.,* vol. 17, pp. 38-45, 1972.

[2] Y. Raitses, D. Staack, M. Keidar, and N. J. Fisch, *Phys. of Plasmas,* no. 12, p. 057104, 2005.

[3] J. M. Haas and A. D. Gallimore, *Physics of Plasmas 8, 652 (2001),* vol. 8, p. 652, 2001.

[4] G. Kornfeld, N. Koch, and H. P. Harmann, in *IEPC-2007-108*, Florence, Italy, 2007.

[5] R. A. Martinez, W. A. Hoskins, P. Y. Peterson, and D. Massey, Ann Arbor, Michigan USA, 2009, IEPC-2009-120.

[6] D. D. Palmer and M. L. R. Walker, *J. Propul. Power,* vol. 25, no. 5, p. 1013, 2009.

[7] E. Y. Choueiri, *J. Prop. and Power,* vol. 14, pp. 744-753, 1998.

[8] M. D. West, C. Charles, and R. W. Boswell, *J. Propul. Power,* vol. 24, p. 134, 2008.

[9] C. Charles, *J. Phys. D: Appl. Phys.,* vol. 42, p. 163001, 2009.

[10] S. Shinohara, H. Nishida, T. Tanikawa, T. Hada, I Funaki, and K. P. Shamrai, *IEEE Trans. Plasma Sci.,* vol. 42, p. 1245, 2014.

[11] K. Takahashi, A. Komuro, and A. Ando, *Plasma Sources Sci. Technol.,* vol. 25, p. 055004, 2015.

[12] A. Grill, Cold Plasma in Materials Fabrication, N. Y.: IEEE Press, 1994.

[13] M. A. Lieberman and A. J. Lichtenberg, Principles of Plasma Discharges and Materials Processing., 2nd ed., N. Y.: Wiley, 2005.

[14] R. L. Boxman, P. J. Martin and D. M. Sanders, Eds., Handbook of Vacuum Arc Science and Technology: fundamentals and applications, N. J.: Noyes Publ., 1995.

[15] E. Dullni, E. Schade, and W. Shang, *IEEE Trans. Plasma Sci.,* vol. 31, pp. 60 - 66, 2002.

[16] T. W. L. Sanford, al., et., *Phys. Rev. Lett.,* vol. 77, pp. 5063-5066, 1996.

[17] R. J. Rosa, C. H. Krueger, and S. Shioda, *IEEE Trans. Plasma Sci.,* vol. 19, p. 1180, 1991.

[18] R. Arad, K. Tsigutkin, Y. Maron, and A. Fruchtman, *Phys. Plasmas,* vol. 11, p. 4515, 2004.

[19] C. Charles and R. W. Boswell, *Plasma Sources Sci. Technol.,* vol. 21, p. 022002, 2012.

[20] K. E. J. Burton, "Atmospheric fueled ion engine". Patent 6,145,298,, 2000.

[21] D. B. Go, D. B. Maturana, T. S. Fisher, and S. V. Garimella, *International Journal of Heat and Mass Transfer,* vol. 51, p. 6047, 2008.

[22] C. Kim and J. J. Hwang, *J. Phys. D: Appl. Phys.,* vol. 45, p. 465204, 2012.

[23] W. J. Gregory, C. Enloe, G. Font, and T. McLaughlin, in *The 45th AIAA Aerospace Sciences Meeting and Exhibit*, Reno, 2007, AIAA 2007-185.

[24] L. Blackhall, and J Khachan, *J. Phys. D: Appl. Phys.,* vol. 40, pp. 2491-2494, 2007.

[25] G. Makrinich and A. Fruchtman, *Phys. Plasmas,* vol. 16, p. 043507, 2009.

[26] G. Makrinich and A. Fruchtman, *Appl. Phys. Lett.,* vol. 95, p. 181504, 2009.

[27] G. Makrinich, and A. Fruchtman,, *Phys. Plasmas,* vol. 20, p. 043509, 2013.

[28] R. L. Washeleski, J. M. Makela, and King, L., B., in *IEPC*, Houghton, 2009.

[29] T. Trottenberg, T. Richter, and H. Kersten, *Eur. Phys. J. D,* p. 91, 2015.

[30] T. Trottenberg and H. Kersten, *Plasma Sources Sci. Technol.,* vol. 26, p. 055011, 2017.

[31] A. Fruchtman, D. Zoler, and G. Makrinich, *Phys. Rev. E,* vol. 84, p. 025402(R), 2011.

[32] G. Makrinich, D Zoler, and A. Fruchtman, Washington, USA,, October,2013.

[33] N. Hershkowitz and M. H. Cho, *J. Vac. Sci. Technol.,* no. A6, p. 2054, 1988.

[34] Y. Raitses, D. Staack, A. Smirnov, and N. J. Fisch, *Phys. Plasmas,* vol. 12, p. 073507, 2005.

[35] S. A. Cohen, F. Zonca, J. Timberlake, T. Bennett, J. Cuthbertson, W. Langer, and R. Motley, *Rev. Sci. Instrum.,* vol. 61, pp. 3586 - 3591, 1990.

[36] D. Chavers and F. Chang-Díaz, *Rev. Sci. Instrum.,* vol. 73, p. 3500, 2002.

[37] Longmier, B.; Reid, B.; Gallimore, A.; Chang-Díaz, F.; Squire, J.; Glover, T.; Chavers, G.; Bering, E., *Journal of Propulsion and Power,* vol. 25, p. 746, 2009.

[38] I. S.Nedzelskiy, C. Silva, H. Fernandes, P. F Duarte, and C. A. Varandas , *Rev. Sci. Instrum.,* vol. 78, p. 123505, 2007.

[39] H. S. Marks, I. I. Beilis, and R. L. Boxman, *IEEE Trans. Plasma Sci.,* vol. 37, pp. 1332 - 1337, 2009.

[40] T. Trottenberg, A. Spethmann, V. Schneider, M. Stahl, M. Giesenhagen, and H. Kersten,, *Contrib. Plasma Phys.,* vol. 52, pp. 584 -592, 2012.

[41] A. Spethmann, T. Trottenberg, and H. Kersten, *Rev. Sci. Instrum.,* vol. 86, p. 015107, 2015.

[42] N. Meezan, W. Hargus, and M. Cappelli, *Phys. Rev.,* vol. E 63, p. 026410, 2001.

[43] M. A. Lieberman and A. J. Lichtenberg, Principles of Plasma Discharges and

Materials Processing, 2nd ed., N. Y.: Wiley, 2005, p. 78.

[44] A. Fruchtman, *Plasma Chem. Plasma Process,* vol. 34, p. 647–660, 2014.

[45] A. Fruchtman, D. Zoler, and G. Makrinich, in *Proceedings of the 20th International Symposium on Plasma Chemistry*, Philadelphia, USA, 2011.

[46] F. F. Chen and D. Arnush, *Phys. Plasmas,* vol. 8, p. 5051, 2001.

[47] F. F. Chen, *Plasma Sources Sci. Technol.,* vol. 15, p. 773–782, 2006.

This manuscript was accepted by J. Appl. Phys. Click here to see the version of record.

Appendix: The method for deducing the plasma potential, electron temperature and plasma density

This subsection describes how the plasma potential V_p, electron temperature T_e, and plasma density n_i were deduced using V_f, V_{ef} and I_{is} measured by the emissive probe and planar Langmuir probe P1 (see Section IV). The method used here for deducing plasma parameters was described in Ref. [45]. The measured and the deduced quantities are related through:

$$eV_f = eV_p + k_B T_e \psi_n(\delta)$$
$$eV_{ef} = eV_p + k_B T_e \psi_c(\delta) \qquad \text{(A1)}$$
$$I_{is} = 0.6 e n_i A_{p1} \sqrt{k_B T_e / m_i}.$$

Here, $\delta \equiv \lambda_D / a$, λ_D is the Debye length and a is the emissive probe radius. The first relation (for a cold, non-emitting probe) was derived in Refs. [46], [45] where $\psi_n(\delta)$ was calculated. In Figure 2 in Ref. [46] ψ_n was denoted as $-\eta_f$ and was shown as a function of $\xi = 1/\delta$, and in Figure 3 in Ref. [45] $\psi_n(\delta)$ was denoted as $e\Phi_c/T_e$. The second relation (for an emitting probe at the space-charge limit) was derived in Ref. [31], and $\psi_c(\delta)$ was shown there in Figure 4. The functions $\psi_n(\delta)$ and $\psi_c(\delta)$ denote the potential drop between the plasma and a floating probe over the electron temperature for cold and emitting probe respectively as a function of δ. A detailed theoretical model is presented in Refs. [31], [45]. We note that λ_D and therefore also δ are functions of the unknowns n_i and T_e, so that there are three unknowns in Equations (A1): V_p, n_i, and T_e. We solved here for the three unknowns at several locations and for several gas flow rates. In solving the equations, Figure 3 and Figure 4 from Ref. [45] were used to calculate $\psi_n(\delta)$ and $\psi_c(\delta)$ respectively.

This manuscript was accepted by J. Appl. Phys. Click here to see the version of record.

To accurately measure the floating potential, the voltmeter resistance has to be much larger than the sheath resistance $R_{sh} \equiv dV/dI_e$ [47], where V is the potential of the emissive probe and I_e is the electron current from the emissive probe to the plasma. The electron current from the probe to the plasma is [47]

$$I_e = I_{es} \exp\left[-\frac{e(V_p - V)}{k_B T_e}\right], \tag{A2}$$

where I_{es} is the electron saturation current. Taking the derivative of V with respect to I_e, the sheath resistance is obtained as

$$R_{sh} = \frac{k_B T_e}{e I_e}. \tag{A3}$$

The sheath resistance of the emissive probe at the floating potential, when $I_e = I_{is}$, is

$$R_{sh} = \frac{k_B T_e}{e I_{is}}. \tag{A4}$$

The floating potential was measured where $T_e < 30$ eV and $I_{is} > 50$ μA so that the maximal sheath resistance is R_{sh}~600 kΩ. This value is much smaller than the resistance of the digital voltmeter (~10 MΩ), as required.

Figure captions

Fig.1: The Radial Plasma Source and Balance Force Meter. Here, r_a=24 mm, $r_b = 70$ mm, $r_c = 80$ mm, $r_m = 40$ mm, $h = 5$mm, and $c = 20$ mm.

Fig.2: The planar Langmuir probes P1 and P2 and the emissive probe with the probes orientation relative to the ion flow.

Fig. 3: Radial profiles of the floating potentials of the emissive probe, V_f (cold probe, no electron emission) and V_{ef} (hot probe, electron emission at space charge limit), for 13 SCCM and 100 SCCM. In Figures 3 – 10, the discharge current was 1.9 A and the maximal magnetic field intensity on the middle plane was 136 G.

Fig. 4: Radial profiles of the ion saturation current, I_{is}, for various gas flow rates (13, 30, 50 and 100 SCCM).

Fig. 5: Radial profiles of the deduced plasma potential, V_p, for various gas flow rates (13, 30, 50 and 100 SCCM).

Fig. 6: Radial profiles of the deduced electron temperature, T_e, for various gas flow rates (13, 30, 50 and 100 SCCM).

Fig. 7: radial profiles of the deduced plasma density, n_i, for various gas flow rates (13, 30, 50 and 100 SCCM).

Fig. 8: Radial profiles of the deduced radial electric field, E_r, (solid line) for various gas flow rates (13, 30, 50 and 100 SCCM) and of the axial magnetic field, B_z, (dashed line).

Fig 9: Radial profiles of the deduced electron pressure, p_e, for various gas flow rates (13, 30, 50 and 100 SCCM).

Fig 10: The force measured by the BFM, F_{BFM}, the total electric force, F_E, [see Equation (14)], the force due to electron pressure, F_{pe}, and the maximal electric force for collisionless ions, F_{cl}, all versus the gas flow rate.

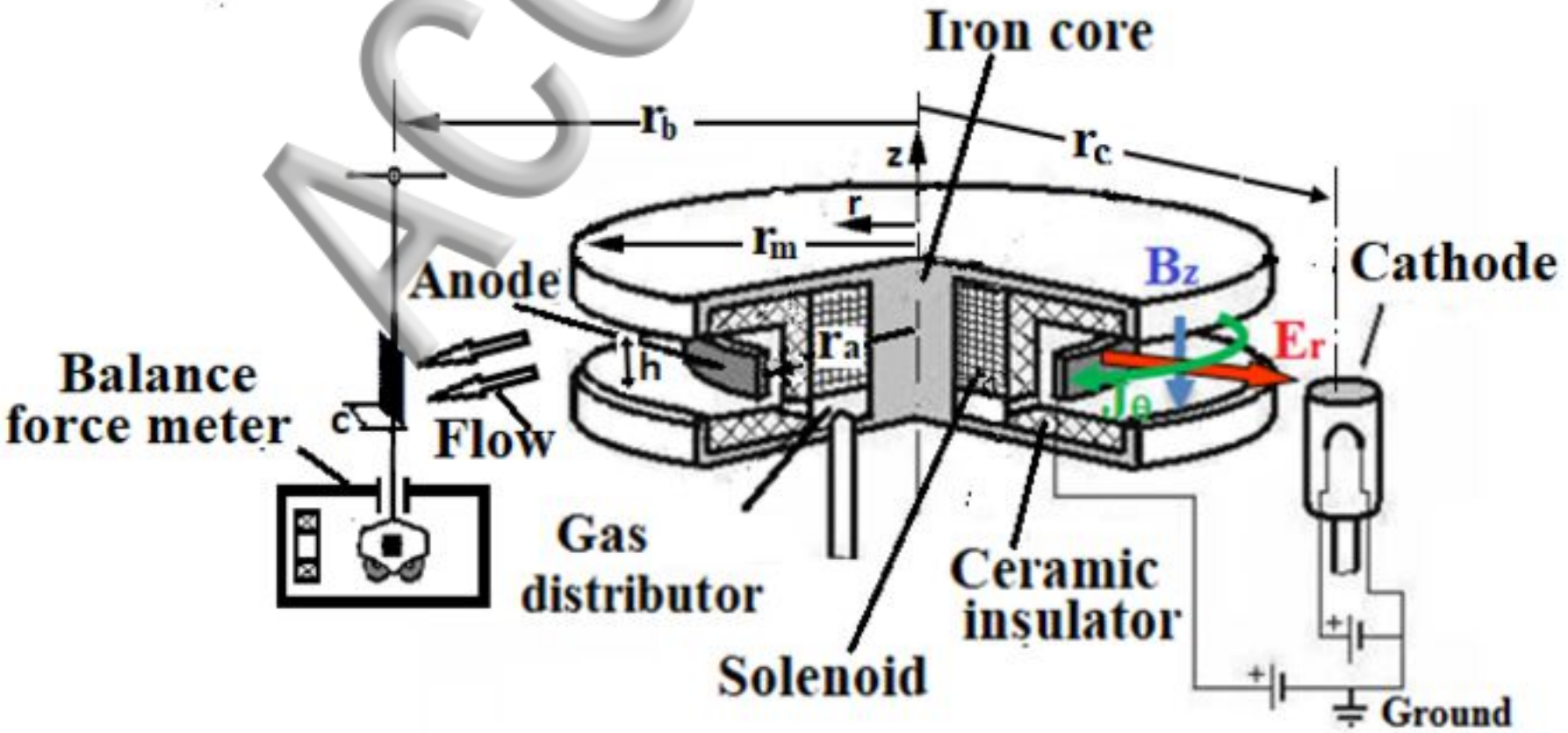
Iron core
r_b
r_c
z
r
r_m
Anode
B_z
Cathode
r_a
h
Er
J_θ
Balance
force meter
Flow
Gas
distributor
Ceramic
insulator
Solenoid
Ground

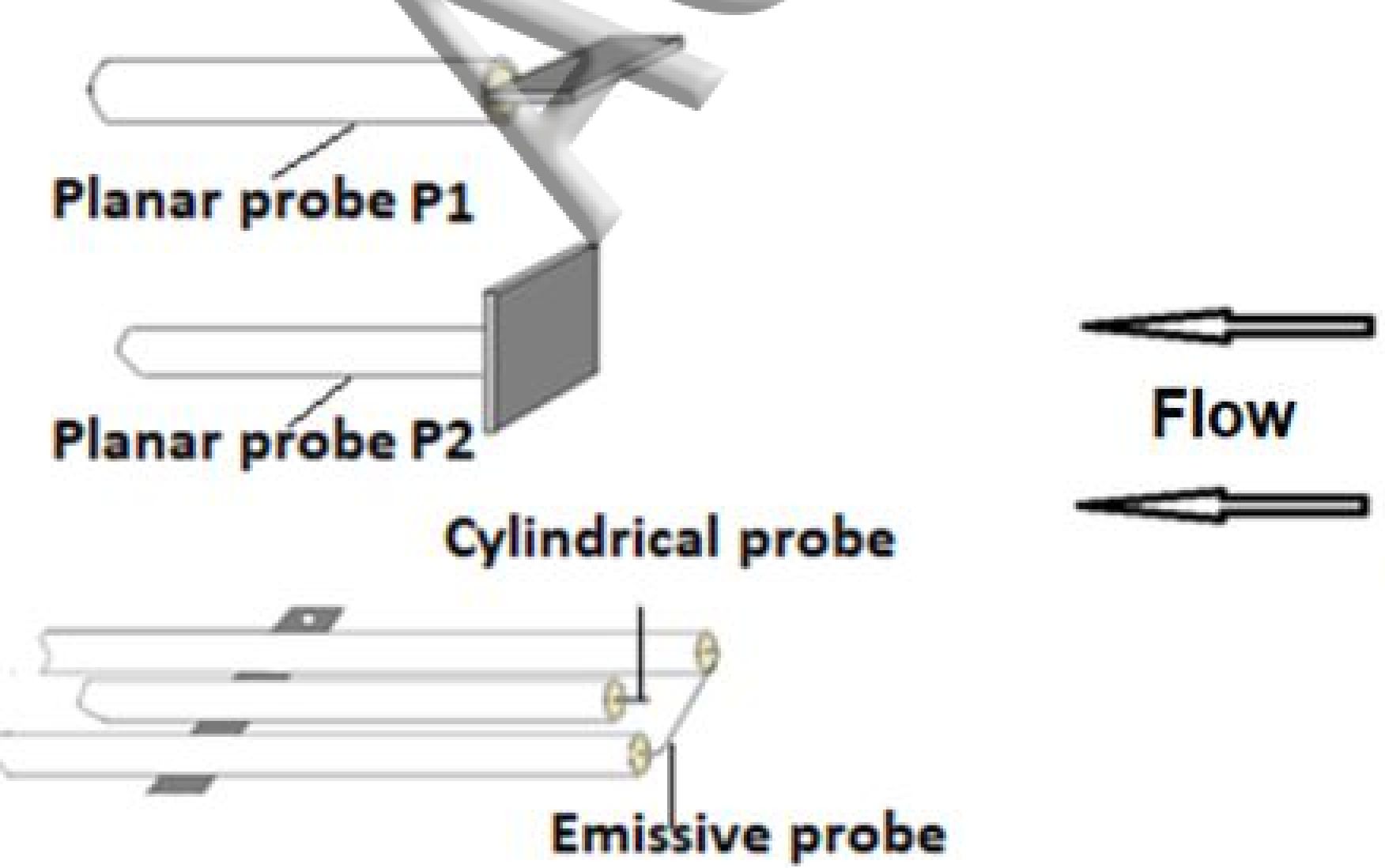
Planar probe P1
Planar probe P2
Flow
Cylindrical probe
Emissive probe

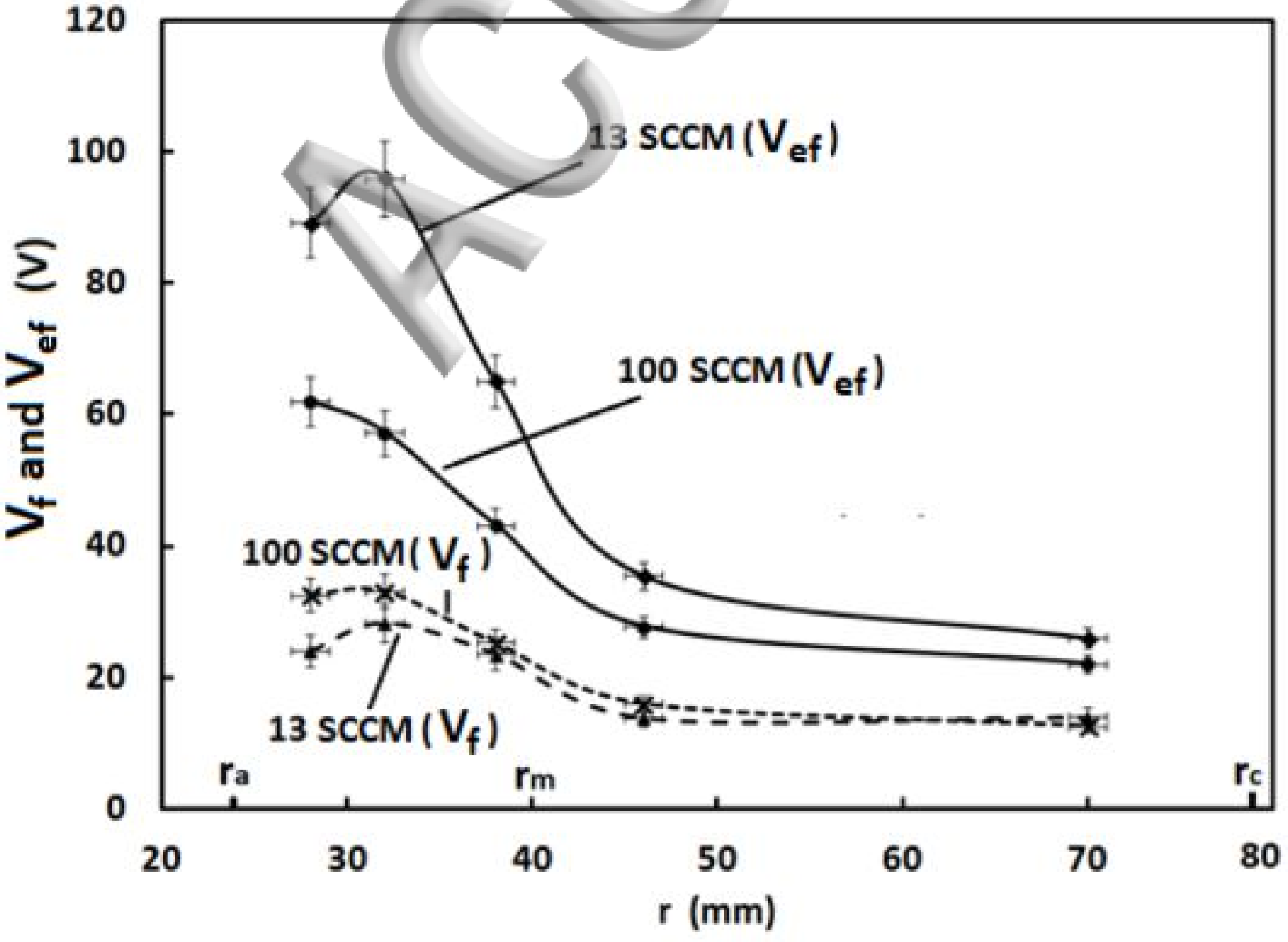
120
100
80
60
40
20
0
V_f and V_{ef} (V)
13 SCCM (V_{ef})
100 SCCM (V_{ef})
100 SCCM (V_f)
13 SCCM (V_f)
r_a
r_m
r_c
20
30
40
50
60
70
80
r (mm)

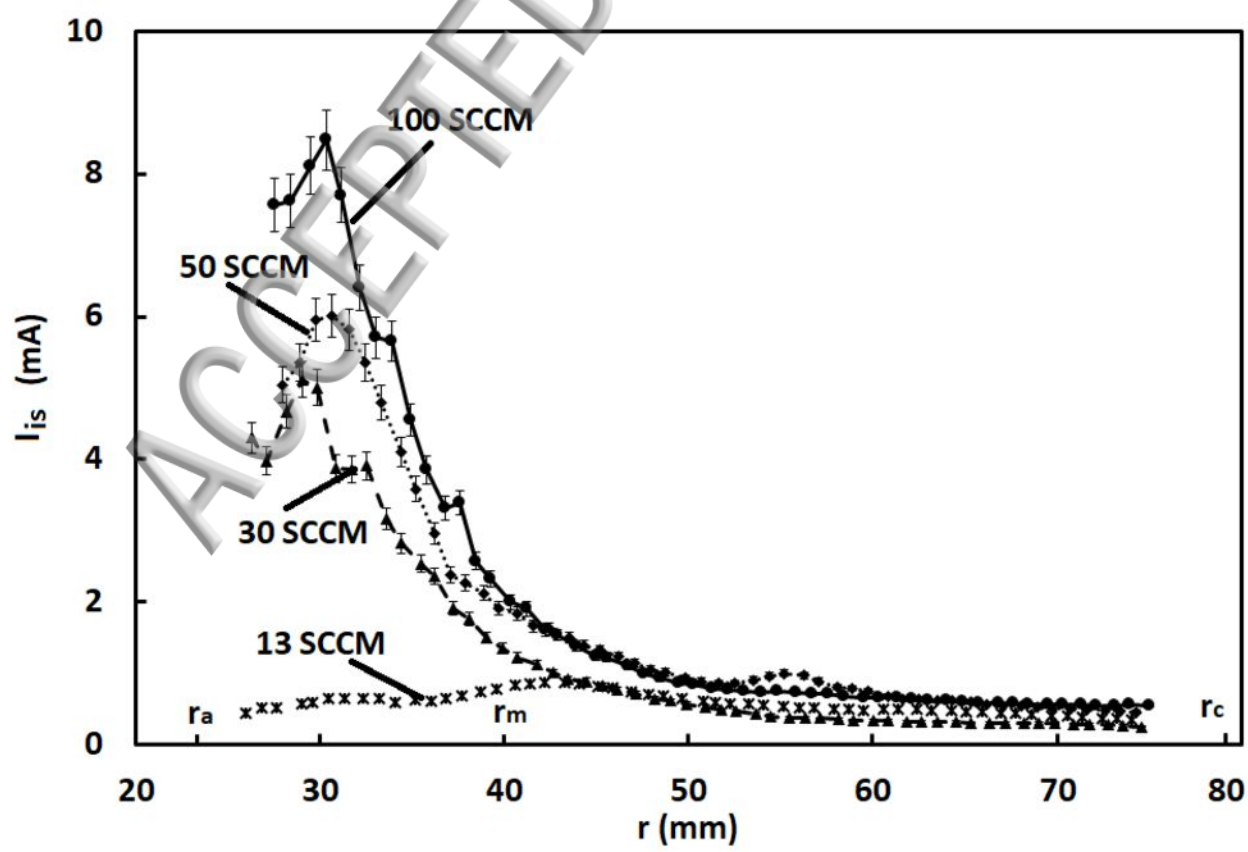
10
8
6
4
2
0
I_{is} (mA)
100 SCCM
50 SCCM
30 SCCM
13 SCCM
r_a
r_m
r_c
20
30
40
50
60
70
80
r (mm)

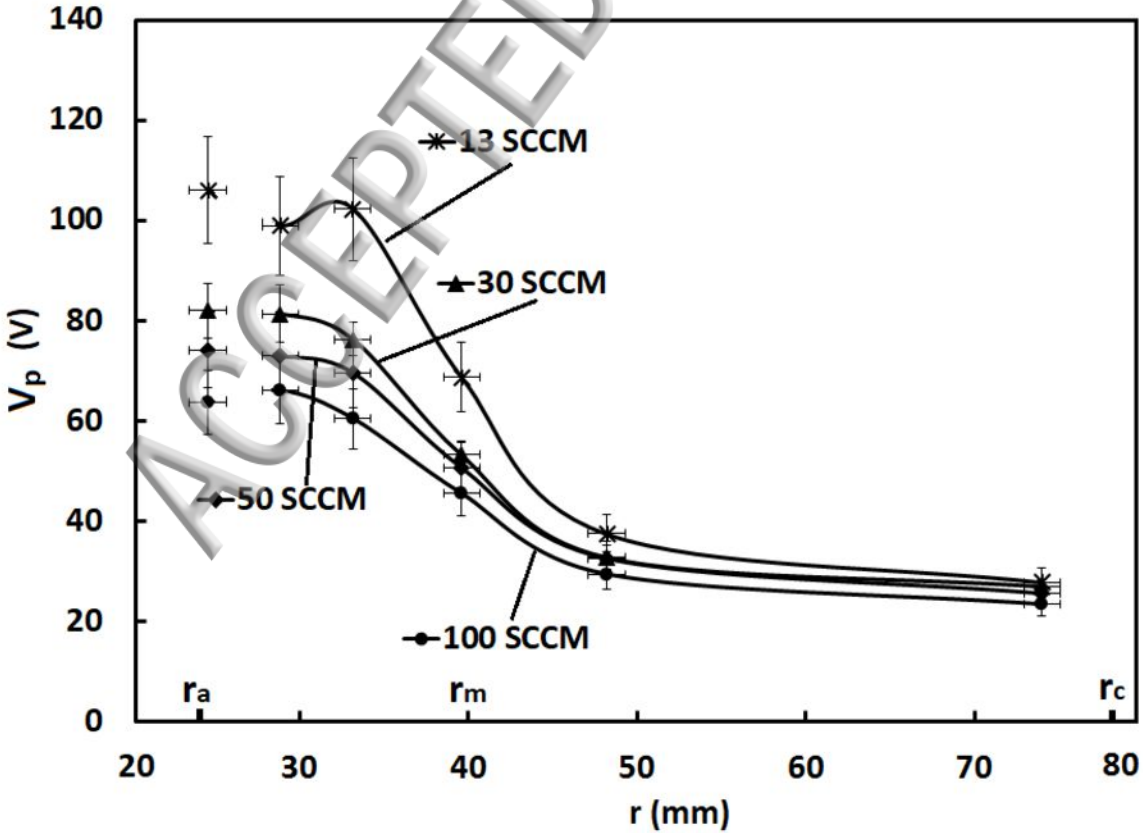
140
120
100
80
60
40
20
0
V_p (V)
13 SCCM
30 SCCM
50 SCCM
100 SCCM
r_a
r_m
r_c
20
30
40
50
60
70
80
r (mm)

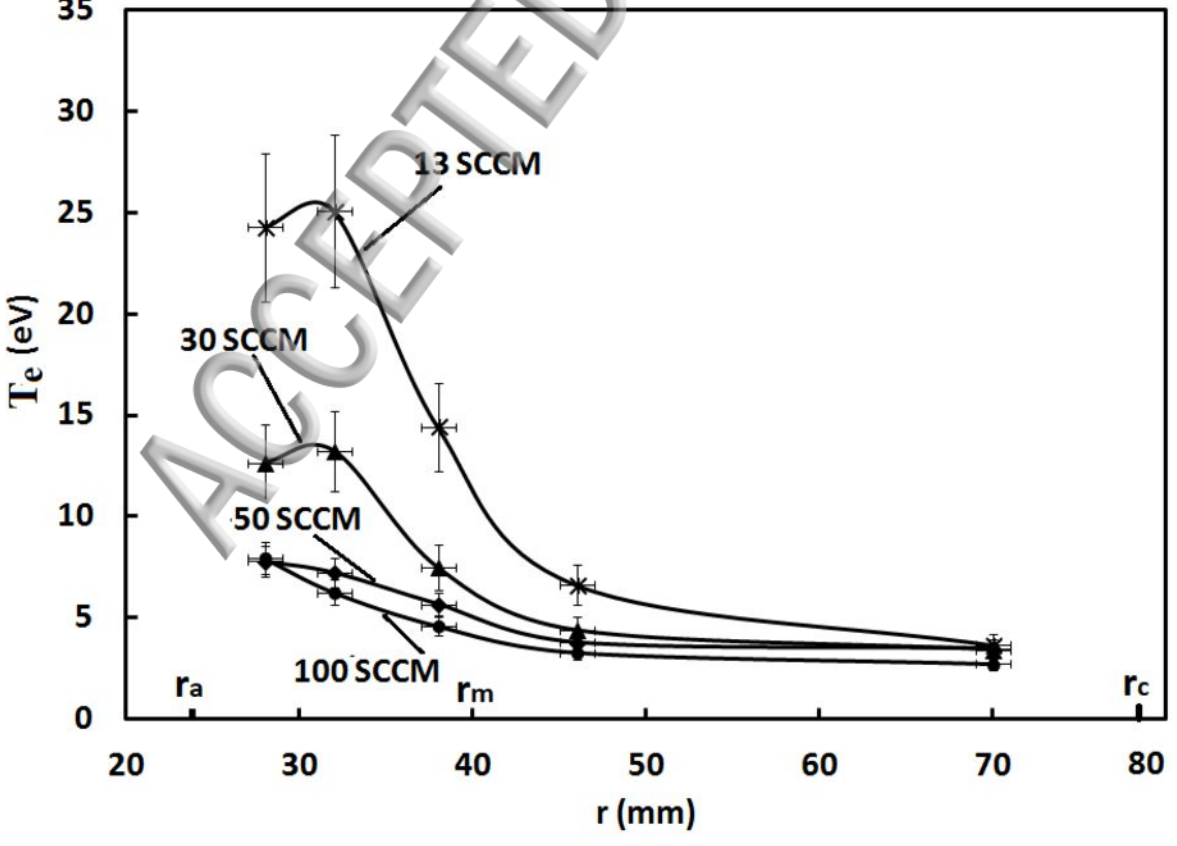
35
30
25
20
15
10
5
0
T_e (eV)
13 SCCM
30 SCCM
50 SCCM
100 SCCM
r_a
r_m
r_c
20
30
40
50
60
70
80
r (mm)

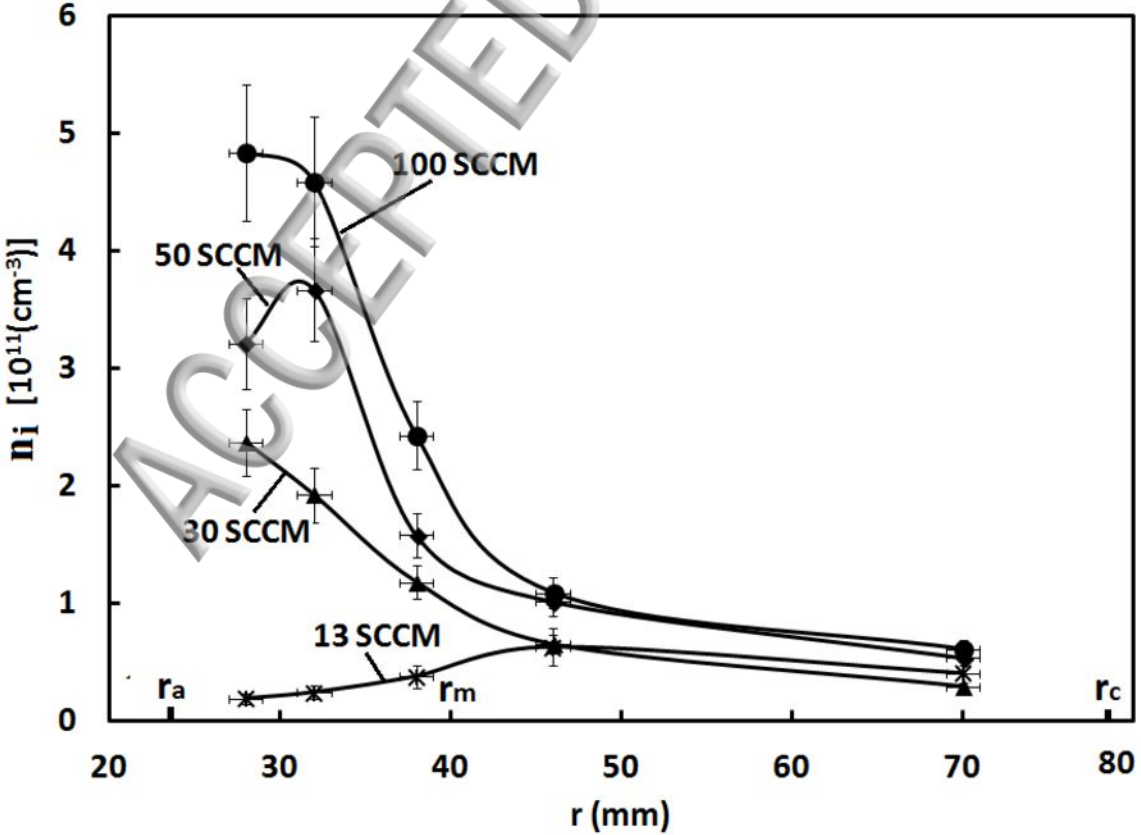
6
5
4
3
2
1
0
n_i [10^{11}(cm^{-3})]
100 SCCM
50 SCCM
30 SCCM
13 SCCM
r_a
r_m
r_c
20
30
40
50
60
70
80
r (mm)

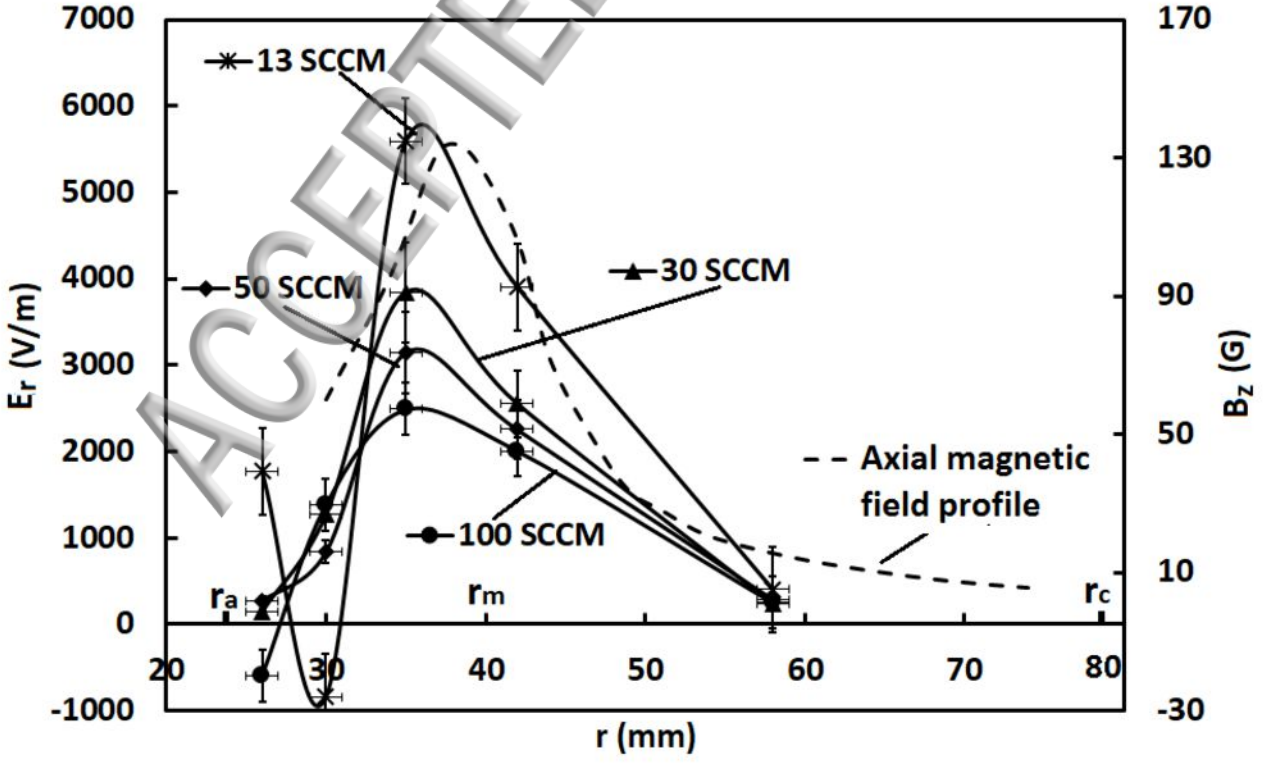
7000
6000
5000
4000
3000
2000
1000
0
-1000
E_r (V/m)
170
130
90
50
10
-30
B_Z (G)
20
30
40
50
60
70
80
r (mm)
13 SCCM
30 SCCM
50 SCCM
100 SCCM
Axial magnetic field profile
r_a
r_m
r_c

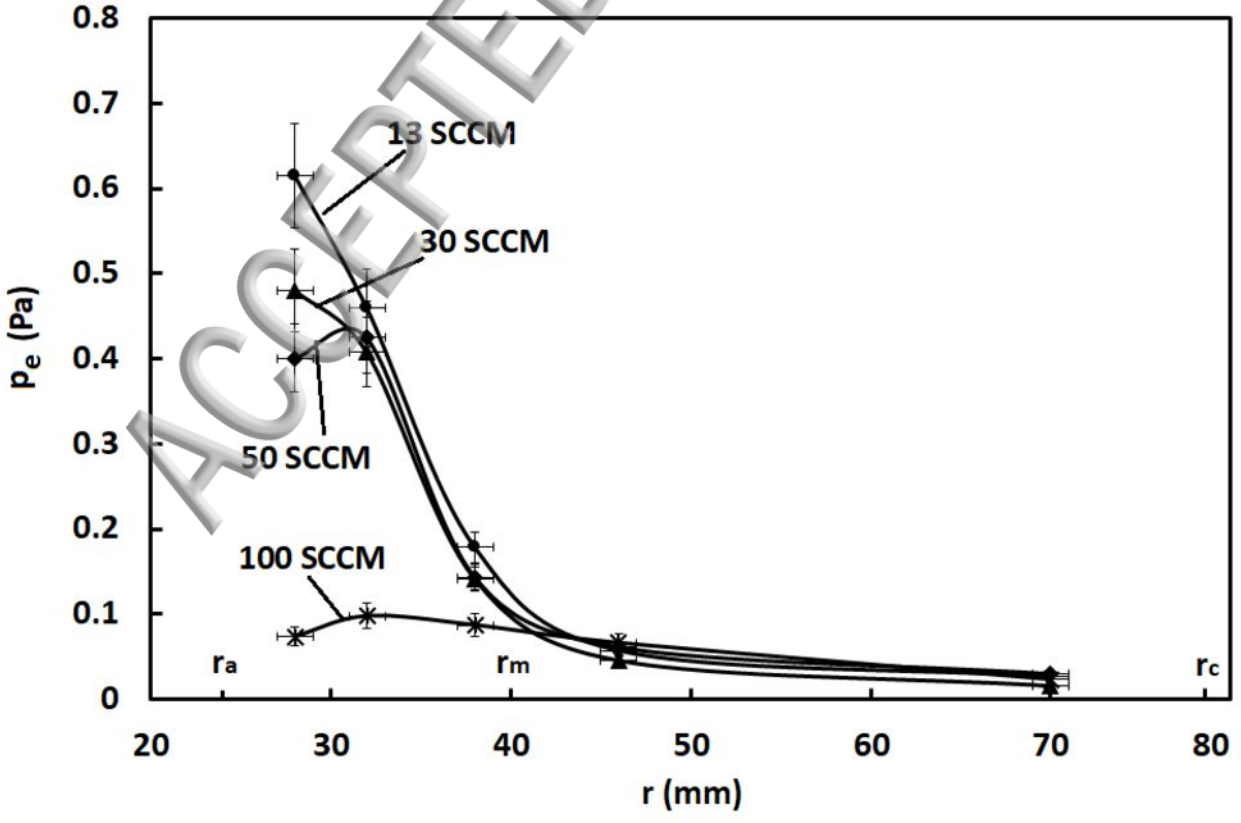
0.8
0.7
0.6
0.5
0.4
0.3
0.2
0.1
0
p_e (Pa)
13 SCCM
30 SCCM
50 SCCM
100 SCCM
r_a
r_m
r_c
20
30
40
50
60
70
80
r (mm)

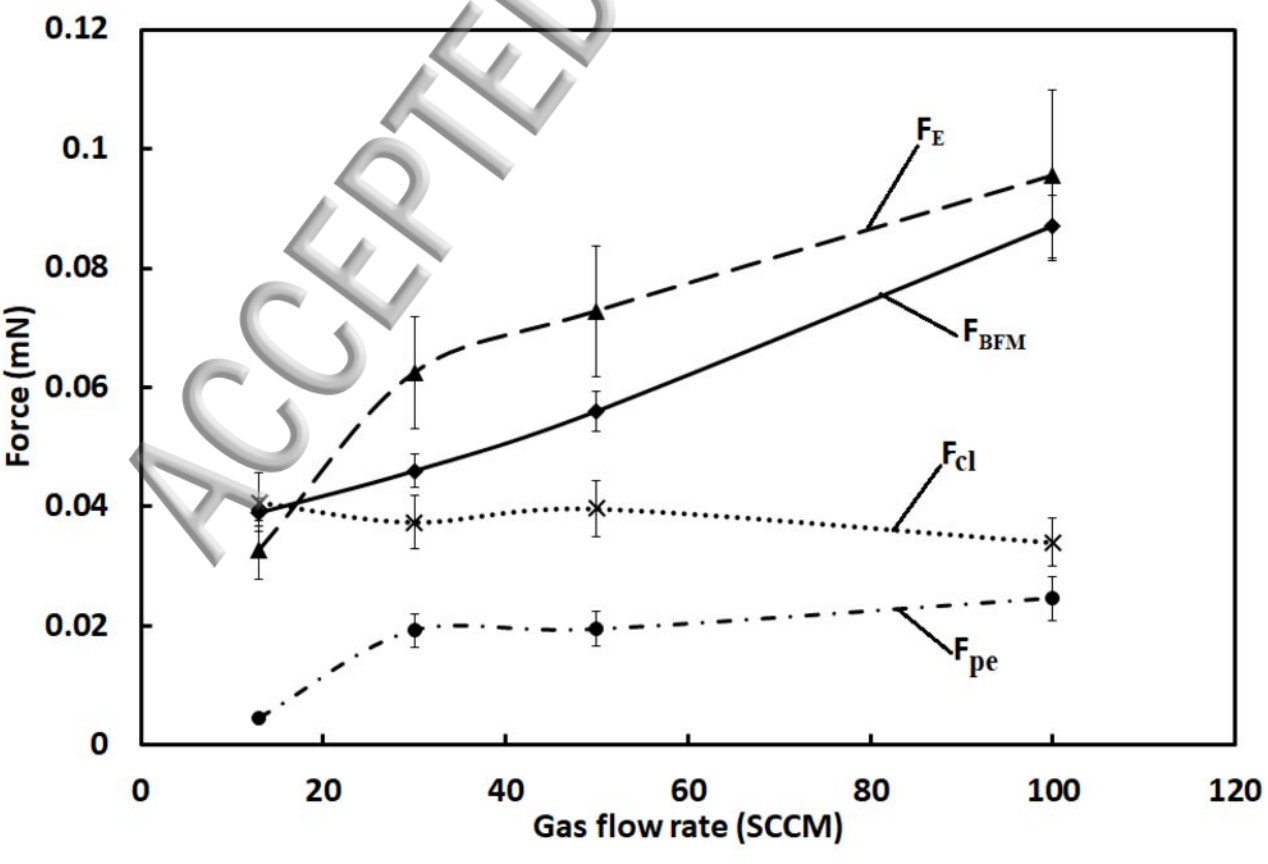
0.12
0.1
0.08
0.06
0.04
0.02
0
Force (mN)
0
20
40
60
80
100
120
Gas flow rate (SCCM)
F_E
F_{BFM}
F_{cl}
F_{pe}